Since January 2020 Elsevier has created a COVID-19 resource centre with free information in English and Mandarin on the novel coronavirus COVID-19. The COVID-19 resource centre is hosted on Elsevier Connect, the company's public news and information website.

Article

Cell Host & Microbe

A Potent Germline-like Human Monoclonal Antibody Targets a pH-Sensitive Epitope on H7N9 Influenza Hemagglutinin

Graphical Abstract

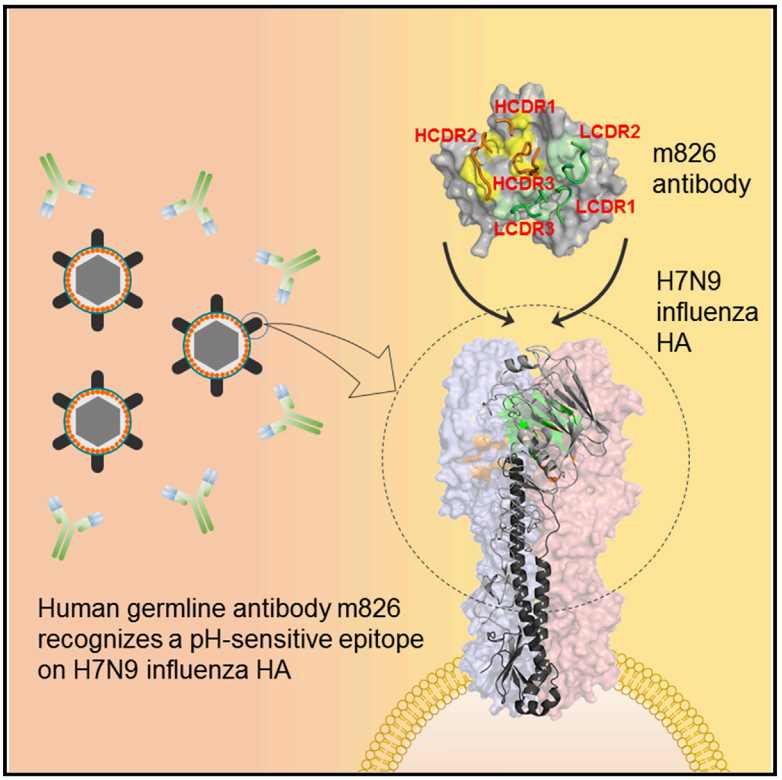

Highlights

- Identification of human germline monoclonal antibody (m826) that binds H7N9 HA
- Structure of H7N9 HA complexed with m826 antibody
- Antibody recognizes a pH-sensitive epitope within H7N9 HA
- Antibody fully protects mice against lethal challenge with H7N9 virus

Authors

Fei Yu, He Song, Yanling Wu, ..., Shibo Jiang, Dimiter S. Dimitrov, Tianlei Ying

Correspondence

tlying@fudan.edu.cn

In Brief

H7N9 influenza virus causes high-mortality disease in humans. Yu et al. identify a human germline monoclonal antibody recognizing a pH-sensitive epitope on H7N9 hemagglutinin globular head. This antibody is effective against H7N9 influenza *in vivo,* likely due to ADCC activity, and may facilitate the development of prophylactics and therapeutics.

Yu et al., 2017, Cell Host & Microbe 22, 471–483
October 11, 2017
http://dx.doi.org/10.1016/j.chom.2017.08.011

CellPress

Cell Host & Microbe
Article

A Potent Germline-like Human Monoclonal Antibody Targets a pH-Sensitive Epitope on H7N9 Influenza Hemagglutinin

Fei Yu,[1,3,8] He Song,[4,8] Yanling Wu,[1,8] So Young Chang,[5] Lili Wang,[1] Wei Li,[2] Binbin Hong,[1] Shuai Xia,[1] Chunyu Wang,[1] Surender Khurana,[6] Yang Feng,[2] Yanping Wang,[2] Zhiwu Sun,[1] Biao He,[1] Dongni Hou,[7] Jody Manischewitz,[6] Lisa R. King,[6] Yuanlin Song,[7] Ji-Young Min,[5] Hana Golding,[6] Xinhua Ji,[4] Lu Lu,[1] Shibo Jiang,[1] Dimiter S. Dimitrov,[2] and Tianlei Ying[1,9,*]
[1]Key Laboratory of Medical Molecular Virology of Ministries of Education and Health, School of Basic Medical Sciences, Fudan University, Shanghai 200032, China
[2]Protein Interactions Section, Cancer and Inflammation Program, Center for Cancer Research, National Cancer Institute, National Institutes of Health, Frederick, MD 21702, USA
[3]College of Life Sciences, Agricultural University of Hebei, Baoding, Hebei 071001, China
[4]Macromolecular Crystallography Laboratory, National Cancer Institute, Frederick, MD 21702, USA
[5]Respiratory Viruses Research Laboratory, Institut Pasteur Korea, Gyeonggi-do 463400, Republic of Korea
[6]Division of Viral Products, Center for Biologics Evaluation and Research, Food and Drug Administration, Silver Spring, MD 20993, USA
[7]Department of Pulmonary Medicine, Zhongshan Hospital, Fudan University, Shanghai 200032, China
[8]These authors contributed equally
[9]Lead Contact
*Correspondence: tlying@fudan.edu.cn
http://dx.doi.org/10.1016/j.chom.2017.08.011

SUMMARY

The H7N9 influenza virus causes high-mortality disease in humans but no effective therapeutics are available. Here we report a human monoclonal antibody, m826, that binds to H7 hemagglutinin (HA) and protects against H7N9 infection. m826 binds to H7N9 HA with subnanomolar affinity at acidic pH and 10-fold lower affinity at neutral pH. The high-resolution (1.9 Å) crystal structure of m826 complexed with H7N9 HA indicates that m826 binds an epitope that may be fully exposed upon pH-induced conformational changes in HA. m826 fully protects mice against lethal challenge with H7N9 virus through mechanisms likely involving antibody-dependent cell-mediated cytotoxicity. Interestingly, immunogenetic analysis indicates that m826 is a germline antibody, and m826-like sequences can be identified in H7N9-infected patients, healthy adults, and newborn babies. These m826 properties offer a template for H7N9 vaccine immunogens, a promising candidate therapeutic, and a tool for exploring mechanisms of virus infection inhibition by antibodies.

INTRODUCTION

Like the highly pathogenic avian influenza A virus subtype H5N1, the avian influenza A virus subtype H7N9 also continues to be a serious threat to public health (Gao et al., 2013). As of May 1, 2017, a total of 1,421 laboratory-confirmed human H7N9 infection cases have been reported (http://www.who.int/csr/don/01-may-2017-ah7n9-china/en/). Most of the cases have been in Mainland China, but the virus has also spread to Hong Kong, Taiwan, Macao, Malaysia, and Canada (Lin et al., 2016). Most seriously, the ongoing fifth epidemic wave represents the largest H7N9 outbreak since its first appearance in 2013, with 693 laboratory-confirmed human infections and much more widespread geographical distributions since October 2016. Currently, however, no approved H7N9-specific vaccine is available to prevent this viral infection, even though some vaccine candidates have entered clinical trials (Tang et al., 2014). In addition, although H7N9 is sensitive to neuraminidase inhibitors, such as oseltamivir (Tamiflu) and zanamivir (Relenza) (Tang et al., 2014; Yen et al., 2013), data from laboratory-scale studies showed that treatment options and possible production of resistant strains may render these influenza antiviral drugs ineffective (Tang et al., 2014; Yen et al., 2013; Kiso et al., 2004). Such findings call for the development of new and effective therapeutic approaches to combat human H7N9 infections.

Monoclonal antibodies (mAbs) are being explored as therapeutics against viruses, including human immunodeficiency virus-1 (HIV-1) (Zhou et al., 2010; Huang et al., 2012, 2014), severe acute respiratory syndrome coronavirus (SARS-CoV), and Nipah and Hendra viruses (Zhu et al., 2007; Xu et al., 2013; Geisbert et al., 2014). For influenza virus, hemagglutinin (HA), a trimeric surface glycoprotein, is the primary target for vaccine and antiviral development. HA facilitates virus entry by binding the sialic acid receptors using its globular head region of HA1 subunit, and then undergoes the acid pH-induced conformational change resulting in fusion between the viral and cellular membranes. Notably, the majority of influenza antibodies elicited by immunization or infection are directed against five antigenic sites on HA1 globular head, designated Ca1, Ca2, Cb, Sa, and Sb (Gerhard et al., 1981; Caton et al., 1982; Zuo et al., 2015). Recently, a number of neutralizing and non-neutralizing mAbs targeting stem region of HA2 were identified that could mediate antiviral effects through Fc-Fcγ receptor interactions

and antibody-dependent cell-mediated cytotoxicity (ADCC) (Kallewaard et al., 2016; DiLillo et al., 2014; Dunand et al., 2016; Tan et al., 2016). However, it remains controversial whether the ADCC effects participate in the functions of HA1-targeting antibodies (Jegaskanda et al., 2014; DiLillo et al., 2014, 2016). Furthermore, an HA1 epitope capable of eliciting protective ADCC-antibodies has not yet been identified (Ye et al., 2017).

In this study, we aimed to develop H7N9 influenza HA1-specific fully human mAbs (hmAbs) with minimal divergence from their germline predecessors. The recombinant H7N9 HA1 and HA proteins were selected as antigens for sequential panning of a very large naive antibody library constructed from the blood of healthy adult donors. Interestingly, one of the selected antibodies, designated as m826, did not neutralize the virus in tissue cultures, but rather, it induced very strong ADCC activity and was highly effective against H7N9 virus infection in a mouse model. It bound to HA with pH-dependent high affinity to a unique epitope distinct from the conventional HA1 antigenic sites as identified by the high-resolution (1.9 Å) crystal structure of its complex with H7N9 HA1. Another unique feature of m826 is its germline sequence which suggests that vaccines based on its epitope could be highly effective, and that its further development as candidate antiviral agents could be easier compared with highly somatically mutated antibodies.

RESULTS

Generation of mAbs

Using peripheral blood B cells from healthy donors, we previously prepared a large phage-displayed antibody Fab library and used it for panning against a number of viral and cancer-related targets (Ying et al., 2014a, 2015; Feng et al., 2016; Puligujja et al., 2015). In this study, we designed a sequential panning strategy to isolate H7N9 HA1-specific antibodies. The antibody library was first panned against baculovirus-expressed HA from the A/Shanghai/1/2013 H7N9 isolate (HA-SH1) and then panned against Fc-fused HA1 from the A/Shanghai/2/2013 isolate (HA1-SH2) for four more rounds (Figure 1A). Significant enrichment against HA-SH1, HA-SH2, and HA1-SH2 was observed after the fourth round of panning (Figure 1B). A panel of antibodies was selected, and one antibody, designated as m826, bound potently to H7 HA proteins (H7N7 and H7N9). m826 was also reactive to H15N8 HA, although to a lesser extent, but not to HA from other subtypes including H1N1, H3N2, H5N1, and H10N8 (Figure 1C).

We next analyzed the sequence of m826 using the IMGT tool to determine its closest VH and VL germline genes. Interestingly, we found that the m826 VH gene shared 100% identity with the IGHV1-69*01 germline, including identical framework and heavy-chain complementarity-determining region (HCDR) 1 and 2 genes (Figure 1D). The m826 VL gene was also very close to IGKV1-39*01 germline (99.6% identity), except for a point mutation, leading to a change from Met to Leu at position 4, which is located in the N terminus of light chain (Figure 1D). The reversion of this mutation (L4M mutant) did not have any effect on the antigen binding of m826 (Figure S1). In fact, while IGKV1-39 and some IGKV alleles have a methionine at position 4, all other alleles (IGKV1-9, IGKV1-13, IGKV1D-13, IGKV1-37, IGKV3-11, IGKV3D-11, IGKV3-20, IGKV3D-20, IGKV5-2, IGKV6-21, IGKV7-3, etc.) have a leucine at this position, suggesting that the point mutation of m826 light chain at position 4 was due to allelic polymorphism rather than somatic mutation.

Immunogenetic Analysis

It is notable that the IGHV1-69 gene was dominantly used by a number of antiviral antibodies, including those targeting influenza viruses, HIV-1, SARS-CoV, and Middle East respiratory syndrome coronavirus (MERS-CoV), among others (Ying et al., 2015; Huang et al., 2004; Pappas et al., 2014; Lingwood et al., 2012; Prabakaran et al., 2012). To further investigate the immunogenetic characteristics of m826-like antibodies, we analyzed in detail the IGHV1-69 recombination frequency with specific IGHD and IGHJ genes using next-generation sequencing data of our antibodyome studies from naive immunoglobulin M (IgM) repertoires of 33 healthy adult donors and neonatal IgM repertoires of 10 newborn babies. Our analysis revealed that IGHV1-69 is one of the most frequently used IGHV genes (Figures S2A and S2B). Among a total of 10,498,301 sequences from healthy adult IgM repertoires, 1,063 sequences were found to display m826-like V(D)J recombination (IGHV1-69, IGHD3, and IGHJ1), indicating a relatively high frequency of this specific V(D)J recombination pattern (Figure S2A). The similar recombination frequency was also observed in IgM repertoires of newborn babies, in which 1,527 sequences with m826-like V(D)J recombination were identified from 5,617,227 sequences (Figure S2B). By aligning the m826 sequence with the sequences from IgM repertoires, we successfully identified a number of clones that share high sequence similarity to m826 (Figures 1E and S2C). Remarkably, a sequence that shared 100% identity (including VDJ and junctional residues) with m826 heavy chain was found from IgM repertoires of newborn babies (Figures 1E and S2C). Furthermore, we have previously sequenced the antibody repertoires of 15 H7N9-infected patients (Hou et al., 2016). Although it is not possible to accurately map the frequency of V(D)J recombination due to the limited numbers of B cells obtained from these patients, we still identified a number of sequences sharing a significant degree of similarity with that of m826 (Figures 1E and S2D).

Next, we assessed the potential compatibility of VH/VL pairing in m826 by searching the IMGT database (IMGT/3Dstructure-DB). We found that the same m826-specific VH/VL pairing, IGHV1-69/IGK1-39, also exists in the previously described antibodies including human anti-HIV-1 antibody 47E (Huang et al., 2004), anti-Dengue virus antibody 5J7 (Fibriansah et al., 2015), and anti-NOTCH3 antibody 20358 (Bernasconi-Elias et al., 2016), indicating the immunologically relevant cognate VH/VL pairing type for m826. Taken together, these results revealed the potential of eliciting m826-like germline antibodies by vaccination.

High-Affinity, pH-Sensitive Binding to a Trimeric HA

Influenza HA exists as a homotrimer on the virion surface. To mimic the native HA, we generated a trimeric HA by fusing a trimeric foldon to the C terminus of H7N9 HA. Interestingly, m826 exhibited pH-sensitive binding to HA. It bound trimeric HA with subnanomolar affinity at pH 5.0, while the binding at pH 7.4 was about 10-fold weaker (K_d = 0.8 versus 9.4 nM)

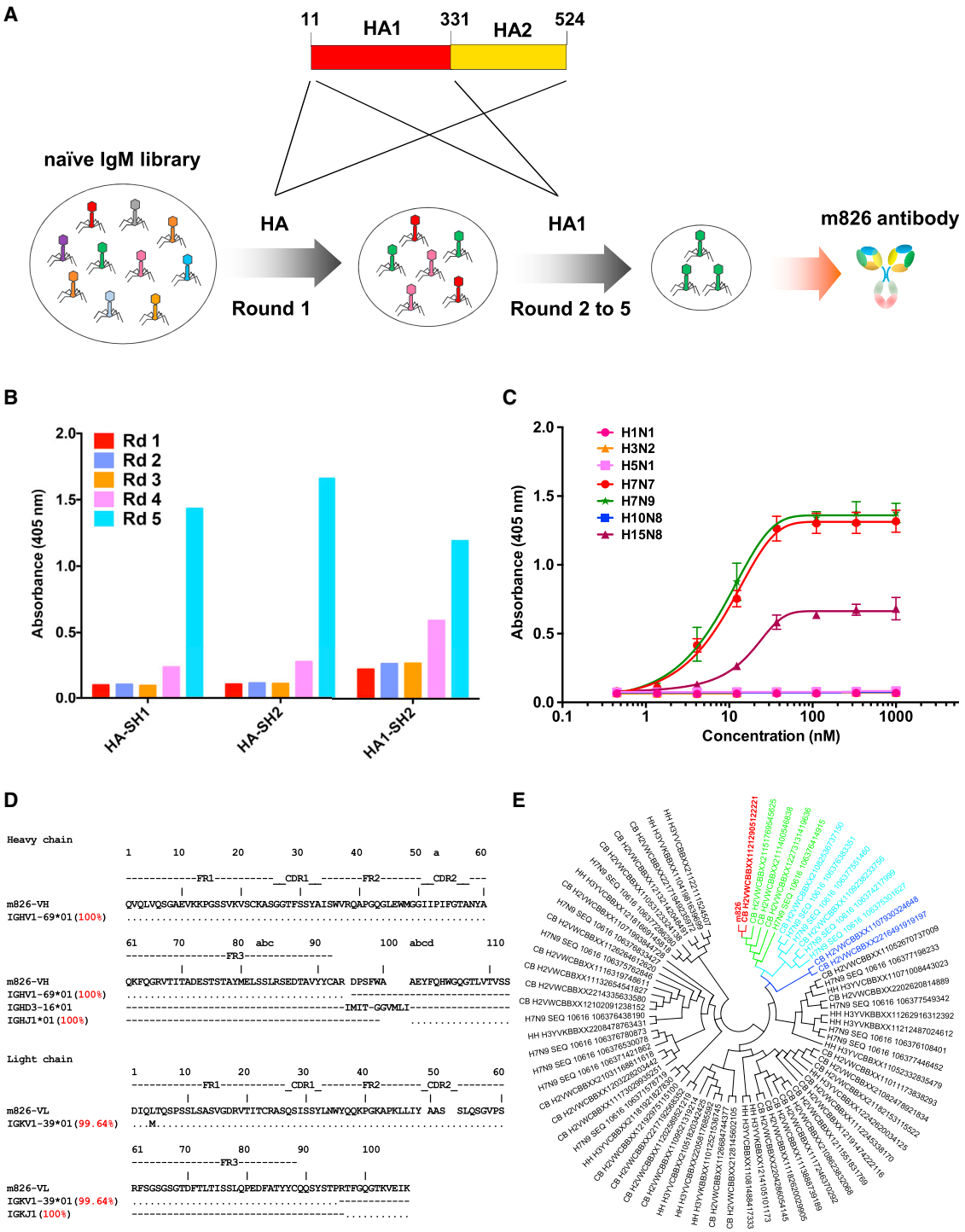

Figure 1. The Schematic Biopanning Process and the Characterization of H7 HA-Specific mAb from the Antibody Library

(A) The biopanning strategy of H7 HA1-specific mAbs from the naive antibody phage display library.

(B) Polyclonal phage ELISA showing the binding of the first to fifth rounds (Rd 1 to Rd 5) of phages to HA and HA1. Bound phages were detected with anti-M13-HRP conjugate.

(C) Binding of Fab m826 to four different subtypes of influenza virus HA. The error bars reflect the SD.

(D) Immunogenetic analysis of the heavy- and light-chain variable regions of m826 using the IMGT tool.

(E) Germline-rooted circular phylogenetic tree of m826-like antibody sequences found in IgM libraries derived from healthy human adults, neonates, and H7N9-infected patients. The sequences of m826 and the clone identical to m826 are shown in red. Sequence ID started with CB represents sequences derived from the neonates, started with HH represents sequences derived from the healthy adults, and started with H7N9 represents that from the H7N9-infected patients. The phylogenetic tree was constructed by the Neighbor-Joining method.

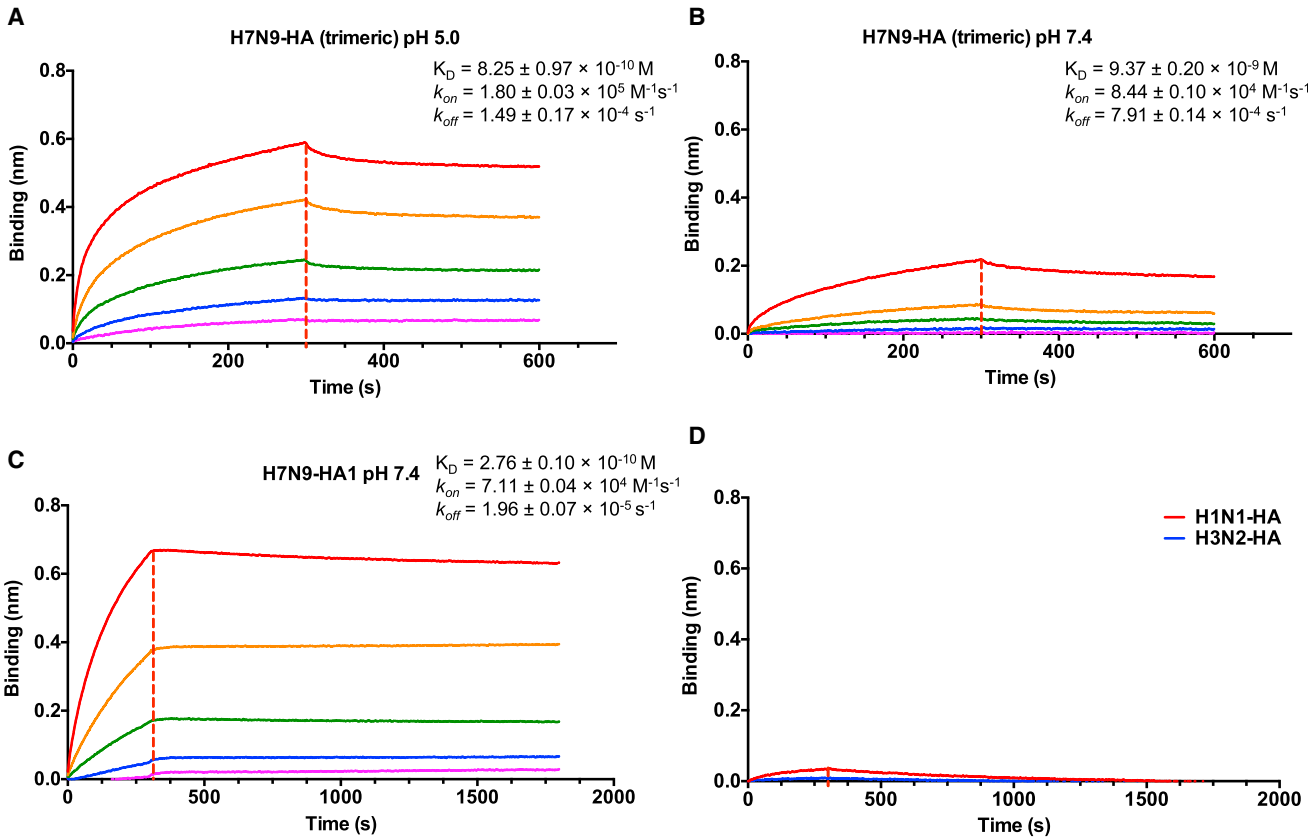

Figure 2. Binding Profiles of m826 mAb to HA and HA1 Measured by BLI in OctetRED96

The m826 mAb was immobilized on activated AR2G biosensors. The analytes consisted of serial dilution (between 100 and 1.2 nM) of trimeric H7N9 HA at pH 5.0 (A) or pH 7.4 (B), H7N9 HA1 at pH 7.4 (C), or 100 nM H1N1 and H3N2 HA at pH 7.4 (D). Binding kinetics was evaluated using a 1:1 Langmuir binding model by ForteBio Data Analysis 7.0 software.

(Figures 2A and 2B). The increased affinity at pH 5.0 resulted from an increase in the on-rate constant (k_{on} = 1.8 × 10^5 versus 8.4 × 10^4 $M^{-1}s^{-1}$) and a decrease in the off-rate constant (k_{off} = 1.5 × 10^{-4} versus 7.9 × 10^{-4} s^{-1}). Interestingly, the binding of m826 with HA1 was not affected by the change of pH, and the binding affinity (0.3 nM) was similar to that of trimeric HA at acidic pH (0.8 nM) (Figure 2C). The m826 showed no binding to H1N1 and H3N2 HA (Figure 2D). These results suggest that m826 recognized a native H7N9 epitope which could be better exposed owing to low pH-induced HA conformational change.

Crystal Structure of Fab m826 in Complex with H7N9 HA1

To map the binding epitope of m826, we determined the crystal structure of Fab m826 in complex with the H7N9 HA1 fragment at high-resolution (1.9 Å) (Figure 3A; Table 1). The overall structure shows that m826 binds to a unique epitope on H7 HA. Consistent with its high binding affinity, the interaction surface buries a total area of about 2,170 $Å^2$. Both the heavy-chain variable domain (V_H) and the light-chain variable domain (V_L) of m826 are involved in the interactions, gripping the antigen with all six CDRs (Figure 3B). At high resolution, the exact contacts at the interface were determined without ambiguity (Figures 3C and 3D). The principal interactions between V_H and HA1 are hydrophobic, with HCDR2 and HCDR3 making extensive contact with the hydrophobic pocket formed by HA1 residues Leu108, Ile111, Trp234, Met236, and Leu260 (Figure 3E; Table S1). Unlike V_H, V_L interacts with HA1 primarily through electrostatic interactions. The LCDR1, LCDR2, and LCDR3 loops were observed to form hydrogen bonds with the hydrophilic residues Lys101, Asn104, Glu106, Gln210, Gln211, and His233 of HA1 (Figure 3E; Table S1).

The receptor-binding site (RBS) of H7 HA is similar to all influenza A virus HA, composing the 130, 150, and 220 loops and 190 helices (Tharakaraman et al., 2013; Xiong et al., 2013). Evidently, the m826 epitope is distinct from the RBS (Figure 4A). In the previously reported H7N9 HA study, HA was purified as a monomer and formed a trimer in the crystallization structure (Yang et al., 2013). Superposition of the HA1 in its m826-bound form with that in trimeric form resulted in Cα root-mean-square deviation of 0.36 Å, indicating that binding of m826 did not induce significant conformational changes. It is interesting to note that the antibody epitope was buried in the trimeric structure (Figure 4B). At acidic pH, HA undergoes conformational changes that lead to the dissociation of the top domains of the trimeric spike and the improved accessibility of m826 epitope, explaining the 10-fold

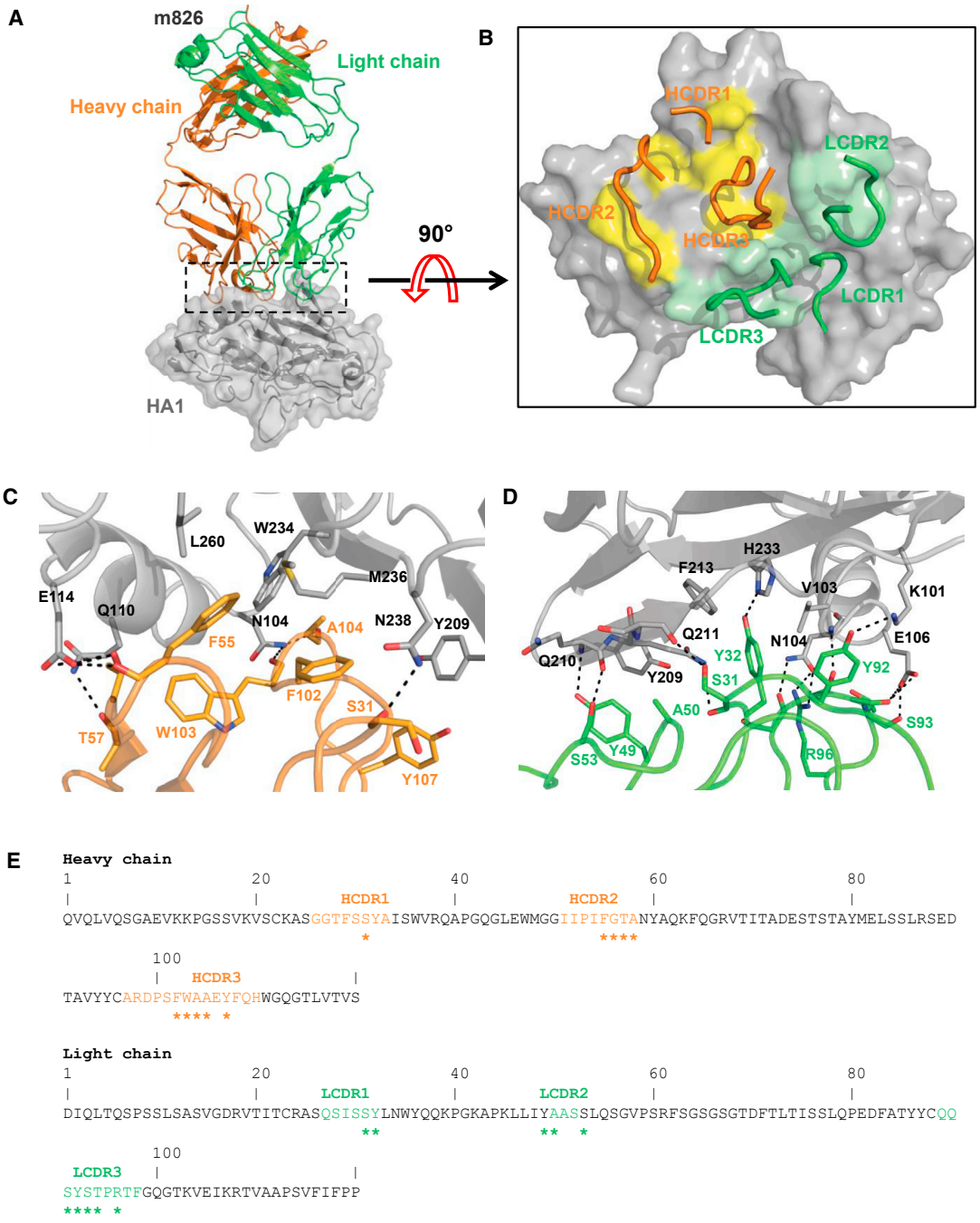

Figure 3. Analysis of Detailed Interactions between the m826 Fab and H7N9 HA

(A and B) The crystal structures of Fab m826 in complex with H7N9 HA1; view from the side (A) and the top (B).

(C) Close-up of the three CDRs of heavy chain from the m826 bound to HA. Side and main chains involved in hydrogen bonding are shown as sticks, with hydrogen bonds depicted as black dotted lines. Residues of the HA protein are labeled. CDR regions are shown as tubes.

(D) The three CDRs of light chain also make direct contacts with HA to form several hydrogen bonds (black dashed lines) with the HA residues.

(E) Amino acid sequences of m826 are shown with Kabat numbering. The CDRs are colored and amino acids involved in HA binding are labeled with *.

difference in binding affinity of m826 to trimeric HA between neutral and acidic pH.

Previous studies have indicated the presence of five conventional antigenic sites on HA1 molecules, including Sa, Sb, Ca1, Ca2, and Cb, which has been extensively characterized using monoclonal and polyclonal mouse antibodies (Gerhard et al., 1981; Caton et al., 1982). These immunodominant antigenic regions correspond to four topographically distinct HA1 regions. We found that the epitope of m826 is distinct from these conventional antibody epitopes (Figure 4C). This epitope is also highly

Table 1. Data Collection and Structure Refinement Statistics

	m826-HA1
Data Collection	
Space group	$P4_12_12$
Cell dimensions	
a, *b*, *c* (Å)	101.3, 101.3, 136.1
α, β, γ (°)	90, 90, 90
Resolution (Å)	40.00–1.90 (1.97–1.90)[a]
R_{pim}	0.092 (0.999)
$I/\sigma I$	29.75 (0.62)
Completeness (%)	97.1 (77.9)
Redundancy	23.6 (7.5)
Refinement	
Resolution (Å)	37.72–1.90
No. of reflections	54,391
R_{work}/R_{free}	0.191/0.229
No. atoms	
Protein	4,997
Ligand/ion	40
Water	414
B factors	
Protein	45.31
Ligand/ion	55.06
Water	49.77
RMSD	
Bond lengths (Å)	0.008
Bond angles (°)	1.01

[a]Values in parentheses are for highest-resolution shell. RMSD, root-mean-square deviation.

conserved among different H7N9 isolates, as well as influenza A virus subtypes H7N7 and H7N4, indicating that m826 recognizes a unique epitope on H7 HA1.

IgG m826 Does Not Neutralize H7 Virus, but Mediates Potent ADCC

In the hemagglutination inhibition (HI) assay, IgG m826 showed weak-to-moderate HI activity against H7N9 with endpoint of 5 μg/mL (Figure S3). We next measured the neutralizing activity of m826 against live H7N3 and H7N9 viruses. Interestingly, while polyclonal sera from immunized rabbits or sheep potently neutralized the viruses, the antibody m826 did not show any neutralization against live H7N3 and H7N9 viruses (Figure S4). To confirm this finding, we further assessed the neutralization of m826 against H7N4 (A/Korea/W266/2007) virus using an imaging-based immunofluorescent assay (Chai et al., 2017). The viral replication was quantified by measuring the level of influenza nucleocapsid protein expression. As shown in Figure 5A, the positive anti-H7N7 control antibody inhibited viral replication approximately 45% at 16 hr post-infection, while m826 did not neutralize H7N4 virus at the same concentration (2 mg/mL). Taken together, these results indicate that m826 cannot effectively neutralize H7 viruses. We also monitored whether m826 interferes with either viral attachment (E_B) to cell surface receptor of target cells or membrane fusion (E_F). R18/SP-DiOC$_{18}$(3)-labeled H7N4 virus was incubated with m826 and applied to A549 cells for 30 and 180 min to examine viral attachment and membrane fusion, respectively. At 30 min post-infection (mpi), we monitored labeled viruses (red dots) in the cells. The viruses incubated with m336 or m826 still entered the cells, while the labeled viruses in a neuraminidase-treated control was significantly decreased (Figure S5A). Moreover, in the entry-fusion assay at 180 mpi, DiOC$_{18}$ signals were detected not in the positive control bafilomycin A1 (Baf-A1) but in the antibody-treated group. Similar to control MERS-CoV antibody m336, neither cell binding nor membrane fusion of the H7N4 virus was affected by IgG m826 (Figure S5B).

We next assessed whether IgG m826 could elicit H7-specific ADCC effect. m826 exhibited strong binding to cells expressing H7N9 HA, as visualized by confocal microscopy (Figure 5B). The ADCC activity was measured in two assays: a dual-luciferase reporter gene-based ADCC assay, and the conventional peripheral blood mononuclear cell (PBMC)-based cytotoxicity assay. CR9114, a potent human mAb targeting a highly conserved epitope in the HA stem (Dreyfus et al., 2012), was used as the positive control. As shown in Figure 5C, m826 elicited robust ADCC against H7N9 HA-expressing cells, whereas the negative control antibody (unrelated anti-MERS-CoV antibody m336) elicited low to undetectable ADCC. It is remarkable that m826 was capable of eliciting evidently higher ADCC activity than CR9114 which has been demonstrated to be a potent mediator of ADCC (Dreyfus et al., 2012; Cox et al., 2016). Similarly, m826 was found to mediate more potent ADCC effect than CR9114 in a concentration-dependent manner using human PBMCs as effector cells (Figure 5D).

Potent Prophylactic and Therapeutic Activity of IgG1 m826 in a Mouse Model of H7N9 Infection

To explore the prophylactic efficacy of m826, BALB/c mice were treated via the intraperitoneal route with two different doses of antibody: 1 and 0.5 mg per mouse. The antibody used in this study was in human IgG1 backbone. After 12 hr, the mice were challenged intranasally with 50 μL lethal doses (10 × LD_{50}) of H7N9 virus. Clinical manifestations (weight loss) and mortality in the mice were monitored for 14 days. As shown in Figure 6A, mice in the control group (PBS) all died 6 days after viral challenge. In contrast, IgG1 m826 at 1 mg conferred full protection (100%) from lethality by H7N9 in the infected mice, while m826 at 0.5 mg per mice was only partially (80%) protective for the mice. Similarly, mice in the control group gradually lost weight after H7N9 infection and eventually died (Figure 6B). Although mice receiving m826 at 1 mg also showed a gradual weight loss after infection, body weight started to recover 4 days post-infection and even increased by the study's end (Figure 6B). Mice receiving m826 at 0.5 mg group lost approximately 20%–30% of body weight until day 9 before starting to recover. Taken together, these results indicate that IgG1 m826 can be highly effective as a prophylactic modality in protecting mice against H7N9 infection and disease.

To evaluate the therapeutic activity of m826 against H7N9 infection, BALB/c mice were infected with 50 μL lethal doses (10 × LD_{50}) of H7N9 virus for 12 hr and then treated via the intraperitoneal route with m826 (1 or 0.5 mg). As shown in Figure 6C, treatment with m826 antibody at 1 mg was able to protect mice

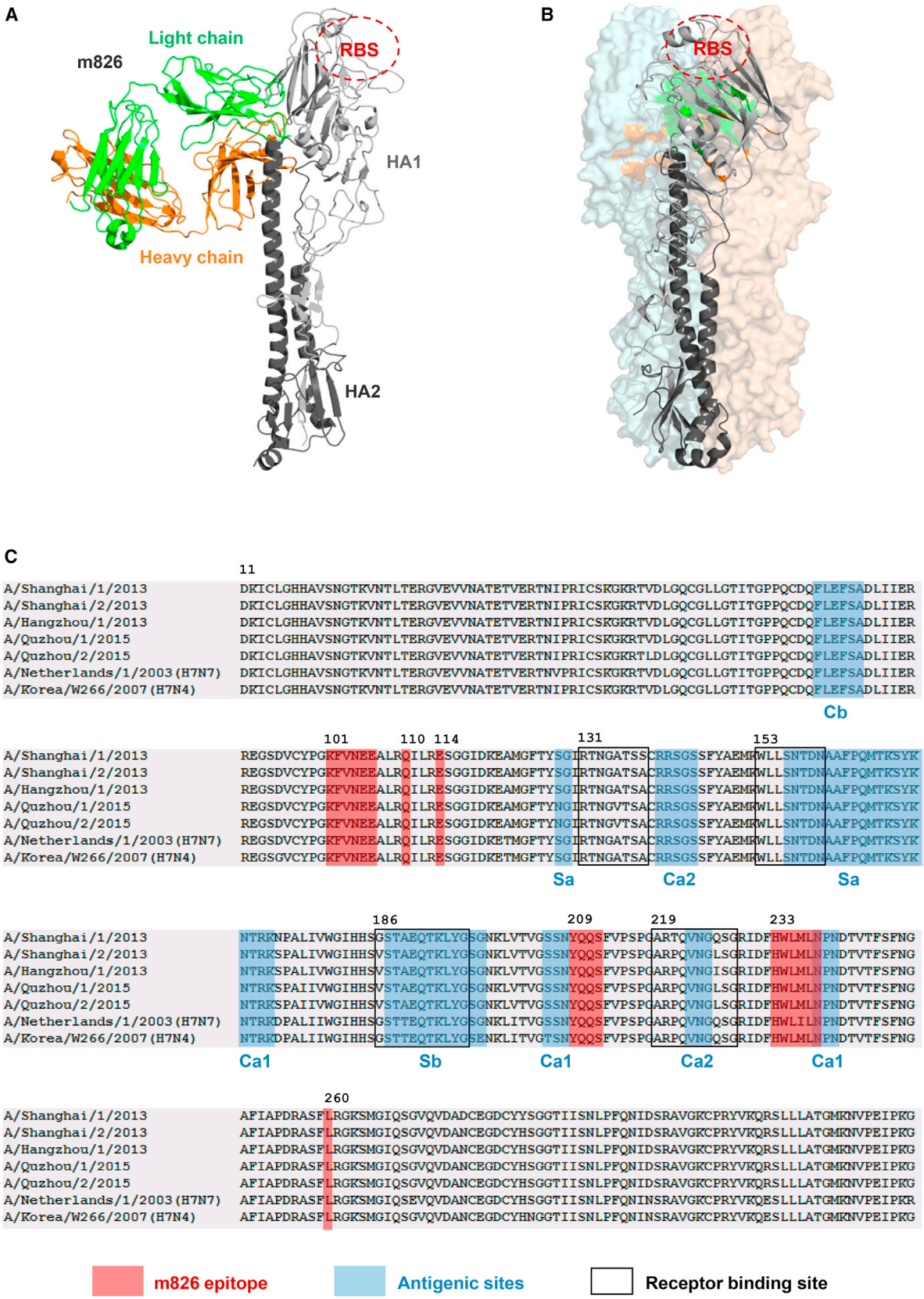

(legend on next page)

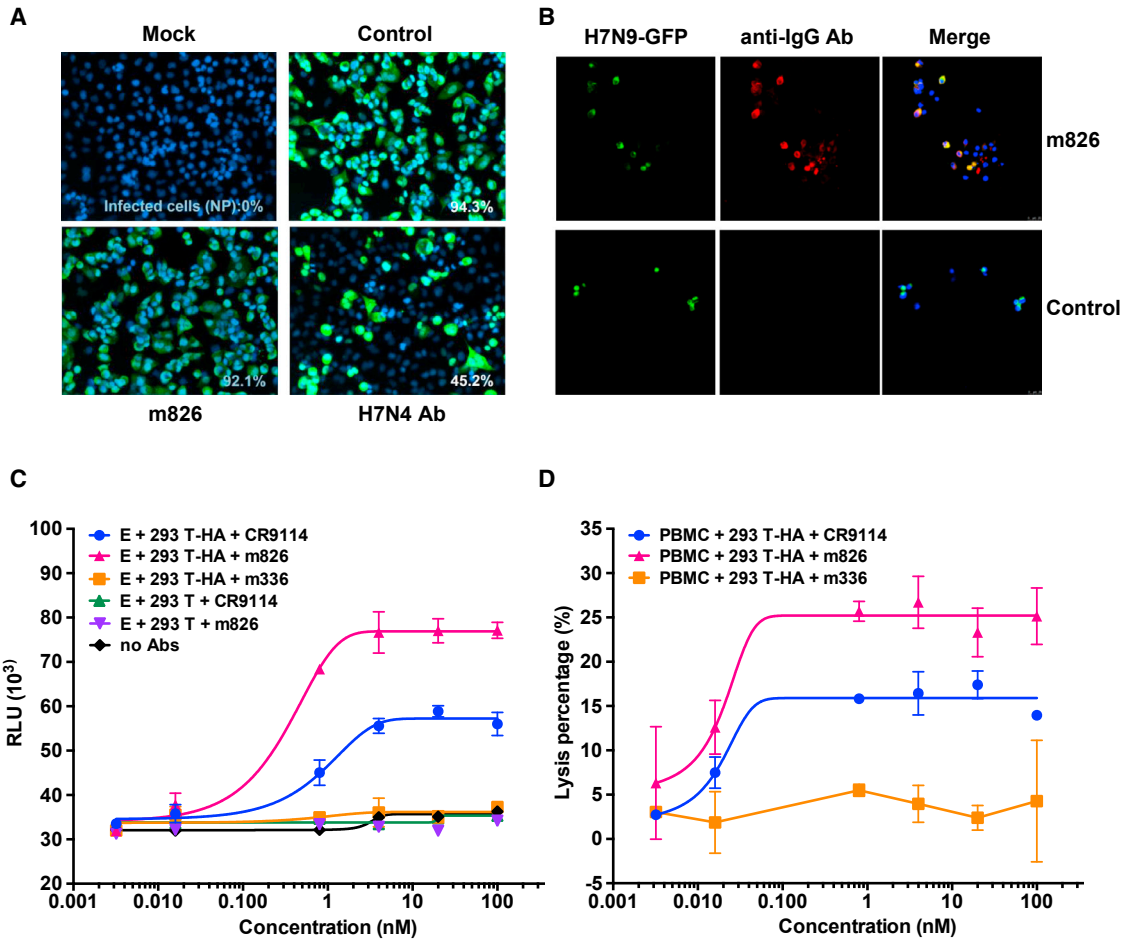

Figure 5. m826 mAb Does Not Neutralize H7 Virus but Mediates Potent ADCC

(A) The immunostaining-based neutralization assay for m826 mAb against H7N4 virus. Immunostaining was conducted using influenza NP-specific mAbs to detect virus-infected cells. H7N4-specfic Ab was used as positive control.

(B) Confocal images of pCMV3-H7N9-HA-GFP transfected 293T cells stained with 100 nM m826 IgG or an unrelated anti-hepatitis B virus human IgG G12 as the control. Green signal, GFP; red signal, detecting with Alexa Fluor 647-conjugated goat anti-human IgG. Scale bar, 25 μm.

(C) ADCC-related signaling in Jurkat T cells engineered to express human FcγRIIIa triggered by m826 and CR9114 IgG in the presence of H7N9 HA-expressing 293T cells. An unrelated anti-MERS-CoV IgG m336 was used as negative control.

(D) ADCC activity of m826 and CR9114 IgG against H7N9 HA-expressing 293T cells mediated by freshly prepared human PBMCs. The percentage (%) of specific lysis was calculated as described in the STAR Methods. All error bars reflect SD.

fully (100%) against the lethality caused by the H7N9 infection. When challenged mice were treated with a low dose of m826 (0.5 mg), 60% of the infected mice survived. Animals in the control group rapidly lost weight (Figure 6D). However, after treatment with m826, all of the infected mice started to recover their body weight at approximately 6–8 days post-infection. These results demonstrated that the ADCC-mediating antibody m826, whether administered as a prophylactic or therapeutic agent, could, like a neutralizing antibody, decrease the mortality and morbidity of mice infected with H7N9.

Treatment with m826 Attenuates Lung Pathology Associated with H7N9 Infection

To explore the lung pathology, one mouse was randomly killed from each group 6 days post-infection. Then the effect of m826 antibody treatment on the pulmonary and bronchial pathology associated with H7N9 infection was evaluated. Compared with the uninfected mice, serious pulmonary interstitial pneumonia was observed in the lung tissues of mice in the control group (Figure 6E). Large amounts of exudate and severe edema with infiltration of lymphocyte cells were also seen. In

Figure 4. m826 mAb Recognizes a Unique Epitope on H7 HA

(A) Docking of the m826-HA1 complex onto the crystal structure of monomeric H7 HA. The epitope of m826 is distinct from the RBS.

(B) Superposition of the antibody epitope which was partially buried in the trimeric HA structure.

(C) Sequence alignment of HA1 from the H7N9, H7N7, and H7N4, and highlighting of structurally defined influenza antibody epitopes. The conventional antigenic sites (Sa, Sb, Ca1, Ca2, and Cb) are shaded in blue, the epitope of m826 is shaded in red, and RBS is shown in the black box.

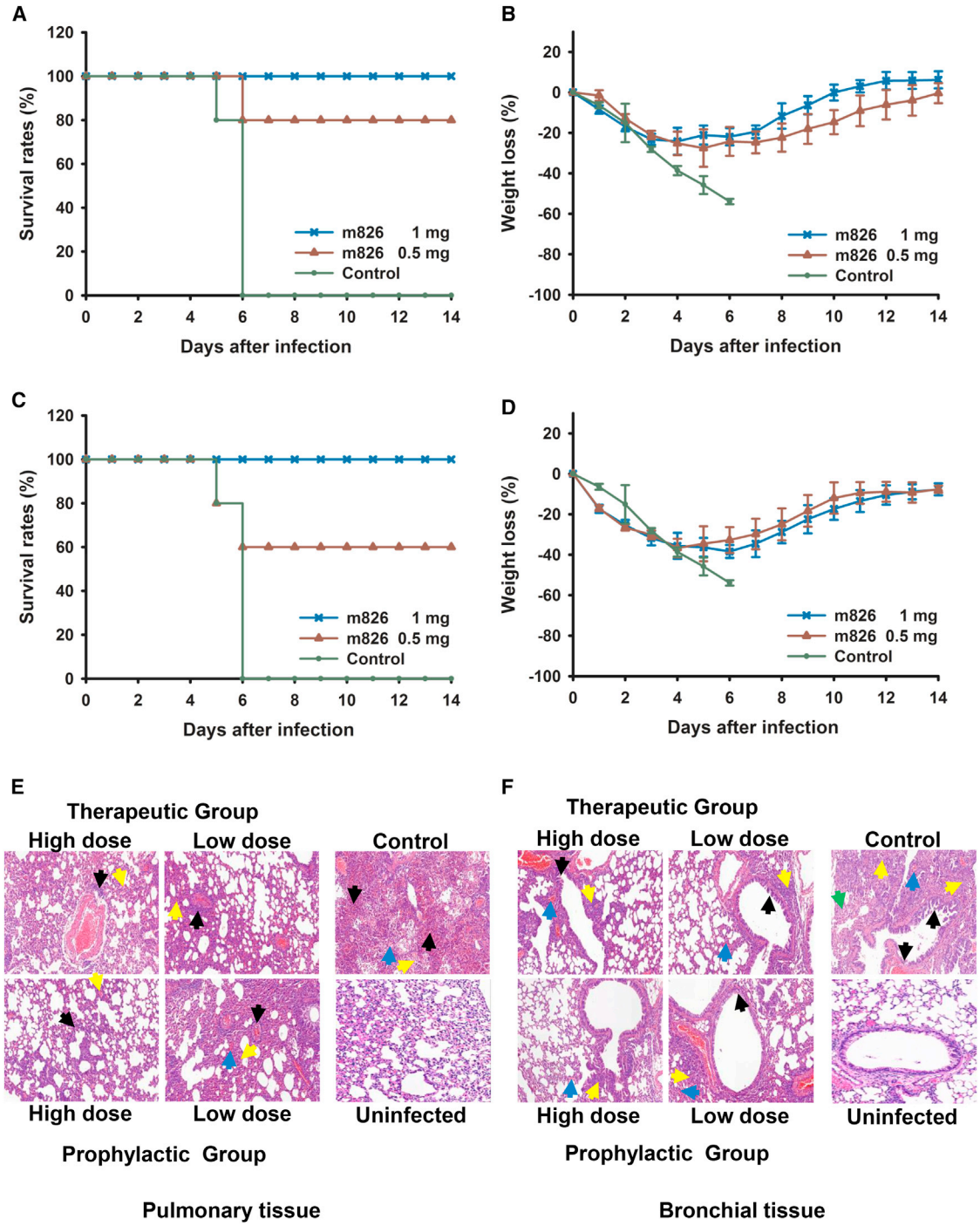

Figure 6. Prophylactic and Therapeutic Efficacy of mAb m826 in Protecting Mice against Lethal Dose H7N9 Challenge

(A–D) For prophylactic efficacy study, mice were treated (intraperitoneally [i.p.]) with m826 antibody 12 hr before viral challenge (intranasally [i.n.]) with 10 × LD_{50} of H7N9 virus and were monitored daily for 14 days for the accumulated mortality (A) and weight loss (B), expressed as percent (%) weight loss and survival, respectively (n = 5 per group). PBS was used for the control group. For therapeutic efficacy study, mice were treated (i.p.) with m826 antibody 12 hr after viral challenge (i.n.) with 10 × LD_{50} of H7N9 virus and were monitored daily for 14 days for the accumulated mortality (C) and weight loss (D). The weight loss of (B and D) represents mean change in body weight per group and SD was also shown.

(E) Evaluation of histopathological changes in the pulmonary tissues of uninfected mice and mice from therapeutic, prophylactic, and control group. The black, yellow, and blue arrows represented the H7N9 infection-induced inflammation of blood vessel, alveoli, or capillary, respectively.

(F) Evaluation of histopathological changes in the bronchial tissues. The black, yellow, blue, and green arrows represented bronchial epithelial cell, bronchial alveoli, capillary, and interstitial tissue, respectively.

contrast, mice that received therapy or prophylaxis with m826 (high or low dose) had mild pulmonary interstitial pneumonia and alveolitis (Figure 6E). Similar results were found in the bronchial tissue. As shown in Figure 6F, bronchial epithelial showed cytopathic effect in the control group, including bronchial epithelial cell degeneration, necrosis, and desquamation. On the contrary, signs of pathology were largely decreased in mice administered with m826 (Figure 6F).

DISCUSSION

H7N9 virus infects humans with high mortality, posing a significant threat to public health and reinforcing the urgency to develop an effective antiviral therapy against H7N9 infection. Therapeutic antibodies have been broadly developed to prevent viral infections, such as licensed antibodies (Keller and Stiehm, 2000) for hepatitis B virus, respiratory syncytial virus, rabies virus, varicella zoster virus, and cytomegalovirus, and developing antibodies for HIV-1, SARS-CoV, MERS-CoV, and Nipah and Hendra viruses (Zhou et al., 2010; Huang et al., 2012, 2014; Geisbert et al., 2014; Xu et al., 2013; Zhu et al., 2007; Ying et al., 2014a; Wang et al., 2015b). Notably, except for isolating mAbs from infected or vaccinated subjects, the large naive antibody library-based technologies have enabled the rapid development of high-affinity hmAbs, highlighting the potential use of antibody-based antivirals against emerging viruses and diseases that occur in an outbreak setting. For instance, by using large naive antibody library, we successfully identified three hmAbs against MERS-CoV, including m336, m337, and m338 (Ying et al., 2014a, 2015). Among them, m336 exhibited the ultrapotent neutralizing activity (half maximal inhibitory concentration [IC_{50}] = 0.005 μg/mL) *in vitro*, and it was also highly effective in three different animal models: rabbit (Houser et al., 2016), mouse (Agrawal et al., 2016), and marmoset (van Doremalen et al., 2017).

In the present study, we identified a human mAb with unique properties that make it a promising candidate therapeutic, as well as a template for vaccine development. Currently, several hmAbs have therapeutic potential to treat H7N9 infection (Henry Dunand et al., 2015; Chen et al., 2015; Tharakaraman et al., 2015; Wang et al., 2015a; Dunand et al., 2016; Thornburg et al., 2016). All these mAbs exhibited comparable activity in mouse models of H7N9 infection. However, their potential for development depends on their respective properties and other factors. This is difficult to predict and requires detailed characterization of a number of properties, including, for example, propensity for aggregation or levels of expression. In general, germline antibodies have better drugability and safety compared with the antibodies with high somatic mutations (Dimitrov, 2010). As one example, our antibody m102.4 against Hendra and Nipah viruses is near germline and exhibited very good drugability, including the successful completion of a phase I clinical trial with 40 healthy volunteers (Zhu et al., 2006, 2008; Bossart et al., 2011; Geisbert et al., 2014). We therefore expect that IgG1 m826 has similarly good drugability as m102.4 and could be further developed as a useful candidate therapeutic.

The germline nature of this antibody also implies that m826, or similar antibodies, can be elicited relatively fast because of the low number of somatic mutations required for affinity maturation. This is in contrast to the antibodies against HIV-1 and likely other chronic infections that could be highly divergent from their putative germline predecessors, and may require extensive and complex affinity maturation pathways to obtain breadth and potency (Zhou et al., 2013; Hoot et al., 2013; Jardine et al., 2013). Indeed, it was recently found that neutralizing mAbs isolated from H7N9 vaccine recipients possessed low numbers of somatic mutations, suggesting the clones arose from naive B cells (Thornburg et al., 2016). Structural analysis suggests that junctional residues play an important role in the binding, which is in agreement with our previous finding that germline-like antibodies achieve high-affinity binding to antigens through V-D and D-J junctional segments and allelic-specific residues (Ying et al., 2015). Because we solved the crystal structure of m826 in complex with the antigen, the structure of the epitope is now known and could be used as a template for a vaccine immunogen which could specifically elicit m826-like antibodies. Such an approach has been used for developing vaccine immunogens against other viruses, including HIV-1 and MERS-CoV, with varying success (Jardine et al., 2013, 2016; Steichen et al., 2016; Bonsignori et al., 2016; Schmidt et al., 2015). It appears that it could be most useful for those viruses typically causing acute infections that elicit antibodies with a relatively low number of mutations, but still capable of potent inhibitory activity.

Interestingly, m826 showed weak-to-moderate HI activity but did not exhibit any neutralization activity against live H7N9 virus. Furthermore, m826 did not interfere with viral attachment or membrane fusion, as indicated by the imaging-based immunofluorescent assay. This could be explained by the unique epitope of m826, which is located opposite to RBS on the head of H7N9 HA. Surprisingly, m826 elicited more potent ADCC than the stem-binding antibody CR9114, contrary to previous findings that anti-stem antibodies and not anti-head antibodies are able to mediate robust ADCC (Cox et al., 2016; DiLillo et al., 2014). It has been recently proposed that optimal antibody-mediated ADCC is dependent on the interaction between influenza HA and sialic acid receptors on immune cells, and thus anti-head antibodies that block sialic acid receptor interactions of HA inhibited FcγRIIIa activation and ADCC elicitation (Cox et al., 2016). In this regard, it is likely that the epitope of m826 was not masked, or even became more exposed, on the binding of HA to sialic acid receptors, allowing the subsequent m826 binding and elicitation of potent ADCC.

Another interesting feature of m826 is the pH dependency of its binding to trimeric HA. The fact that binding of m826 to HA1 was not affected by pH change, and that the binding affinity of m826 to monomeric HA1 was similar to that of m826 to trimeric HA at acidic pH, suggests that the epitope of m826 is sensitive to the conformational change of HA head. According to our *in vitro* assays, such binding apparently does not interfere with viral entry. Nonetheless, more experiments are required before we can identify with certainty whether the better exposure of the m826 epitope could be induced by the binding of HA to sialic acid receptors, and plays a role in the elicitation of potent ADCC by m826.

In conclusion, the identified hmAb m826 appears to exhibit several unique features which could contribute to its use as both reagent for exploring the mechanisms of H7N9 entry into cells and for development of therapeutics and vaccines.

STAR★METHODS

Detailed methods are provided in the online version of this paper and include the following:

- KEY RESOURCES TABLE
- CONTACT FOR REAGENT AND RESOURCE SHARING
- EXPERIMENTAL MODEL AND SUBJECT DETAILS
  - Murine Lethal Challenge Model
  - Cells and Viruses
- METHOD DETAILS
  - Ethics Statement
  - Expression and Purification of Viral HA
  - Antibody Screening from Phage Library
  - Enzyme-linked Immunosorbent Assay
  - Expression and Purification of m826 Fab and IgG Formats
  - Biolayer Interferometry Binding Assays
  - Next-generation Sequencing
  - Crystallization, Data Collection and Structure Determination
  - Hemagglutination Inhibition and Neutralization Assays
  - Cell-based Binding and Viral Entry Assays
  - ADCC Assay
  - Histopathological Analysis
- QUANTIFICATION AND STATISTICAL ANALYSIS
- DATA AVAILABILITY

SUPPLEMENTAL INFORMATION

Supplemental Information includes five figures and one table and can be found with this article online at http://dx.doi.org/10.1016/j.chom.2017.08.011.

AUTHOR CONTRIBUTIONS

T.Y. and D.S.D. conceived, designed, and supervised the project. F.Y., Y.W., S.Y.C., L.W., W.L., B.H., S.X., C.W., S.K., Y.F., Y.W., Z.S., B.H., J.M., L.R.K., J.Y.M., and T.Y. carried out the biochemical experiments. H.S., T.Y., and X.J. determined and analyzed the crystal structure. B.H., D.H., Y.S., and T.Y. analyzed the next-generation sequencing data. T.Y., F.Y., H.S., H.G., L.L., S.J., and D.S.D. integrated all the data and wrote the paper with input from all co-authors.

ACKNOWLEDGMENTS

This work was supported by the National Natural Science Foundation of China (31570936, 81501735, 81561128006), the 1000 Young Talents Program of China, National Key Research and Development Program of China (2016YFC1201000, 2016YFC1200405), the Technology Service Platform for Detecting High-level Biological Safety Pathogenic Microorganisms supported by the Shanghai Science and Technology Commission (15DZ2290200), Open Collaboration Program of MOE/MOH Key Laboratory of Medical Molecular Virology (FDMV-2017004), and the Intramural Research Program, National Cancer Institute, National Institutes of Health. X-ray diffraction data were collected at Southeast Regional Collaborative Access Team (SER-CAT) 22-ID beamline at Advanced Photon Source (APS), Argonne National Laboratory. Supporting institutions may be found at www.ser-cat.org/members.html. Use of the APS was supported by U. S. Department of Energy, Office of Science, Office of Basic Energy Sciences, under Contract No. W-31-109-Eng-38.

Received: May 3, 2017
Revised: July 12, 2017
Accepted: August 22, 2017
Published: September 28, 2017

REFERENCES

Agrawal, A.S., Ying, T., Tao, X., Garron, T., Algaissi, A., Wang, Y., Wang, L., Peng, B.H., Jiang, S., Dimitrov, D.S., et al. (2016). Passive transfer of A germline-like neutralizing human monoclonal antibody protects transgenic mice against lethal Middle East respiratory syndrome coronavirus infection. Sci. Rep. *6*, 31629.

Banerjee, I., Yamauchi, Y., Helenius, A., and Horvath, P. (2013). High-content analysis of sequential events during the early phase of influenza A virus infection. PLoS One *8*, e68450.

Bernasconi-Elias, P., Hu, T., Jenkins, D., Firestone, B., Gans, S., Kurth, E., Capodieci, P., Deplazes-Lauber, J., Petropoulos, K., Thiel, P., et al. (2016). Characterization of activating mutations of NOTCH3 in T-cell acute lymphoblastic leukemia and anti-leukemic activity of NOTCH3 inhibitory antibodies. Oncogene *35*, 6077–6086.

Bonsignori, M., Zhou, T.Q., Sheng, Z.Z., Chen, L., Gao, F., Joyce, M.G., Ozorowski, G., Chuang, G.Y., Schramm, C.A., Wiehe, K., et al. (2016). Maturation pathway from germline to broad HIV-1 neutralizer of a CD4-mimic antibody. Cell *165*, 449–463.

Bossart, K.N., Geisbert, T.W., Feldmann, H., Zhu, Z., Feldmann, F., Geisbert, J.B., Yan, L., Feng, Y.R., Brining, D., Scott, D., et al. (2011). A neutralizing human monoclonal antibody protects African green monkeys from Hendra virus challenge. Sci. Transl. Med. *3*, 105ra103.

Caton, A.J., Brownlee, G.G., Yewdell, J.W., and Gerhard, W. (1982). The antigenic structure of the influenza virus A/PR/8/34 hemagglutinin (H1 subtype). Cell *31*, 417–427.

Chai, N., Swem, L.R., Park, S., Nakamura, G., Chiang, N., Estevez, A., Fong, R., Kamen, L., Kho, E., Reichelt, M., et al. (2017). A broadly protective therapeutic antibody against influenza B virus with two mechanisms of action. Nat. Commun. *8*, 14234.

Chen, Z., Wang, J.M., Bao, L.L., Guo, L., Zhang, W.J., Xue, Y., Zhou, H.L., Xiao, Y., Wang, J.W., Wu, F., et al. (2015). Human monoclonal antibodies targeting the haemagglutinin glycoprotein can neutralize H7N9 influenza virus. Nat. Commun. *6*, 6714.

Cox, F., Kwaks, T., Brandenburg, B., Koldijk, M.H., Klaren, V., Smal, B., Korse, H.J., Geelen, E., Tettero, L., Zuijdgeest, D., et al. (2016). HA antibody-mediated FcgammaRIIIa activity is both dependent on FcR engagement and interactions between HA and sialic acids. Front. Immunol. *7*, 399.

DiLillo, D.J., Tan, G.S., Palese, P., and Ravetch, J.V. (2014). Broadly neutralizing hemagglutinin stalk-specific antibodies require FcgammaR interactions for protection against influenza virus in vivo. Nat. Med. *20*, 143–151.

DiLillo, D.J., Palese, P., Wilson, P.C., and Ravetch, J.V. (2016). Broadly neutralizing anti-influenza antibodies require Fc receptor engagement for in vivo protection. J. Clin. Invest. *126*, 605–610.

Dimitrov, D.S. (2010). Therapeutic antibodies, vaccines and antibodyomes. MAbs *2*, 347–356.

Dreyfus, C., Laursen, N.S., Kwaks, T., Zuijdgeest, D., Khayat, R., Ekiert, D.C., Lee, J.H., Metlagel, Z., Bujny, M.V., Jongeneelen, M., et al. (2012). Highly conserved protective epitopes on influenza B viruses. Science *337*, 1343–1348.

Du, L.Y., Jin, L., Zhao, G.Y., Sun, S.H., Li, J.F., Yu, H., Li, Y., Zheng, B.J., Liddington, R.C., Zhou, Y.S., et al. (2013). Identification and structural characterization of a broadly neutralizing antibody targeting a novel conserved epitope on the influenza virus H5N1 hemagglutinin. J. Virol. *87*, 2215–2225.

Dunand, C.J.H., Leon, P.E., Huang, M., Choi, A., Chromikova, V., Ho, I.Y., Tan, G.S., Cruz, J., Hirsh, A., Zheng, N.Y., et al. (2016). Both neutralizing and non-neutralizing human H7N9 influenza vaccine-induced monoclonal antibodies confer protection. Cell Host Microbe *19*, 800–813.

Echols, N., Grosse-Kunstleve, R.W., Afonine, P.V., Bunkoczi, G., Chen, V.B., Headd, J.J., McCoy, A.J., Moriarty, N.W., Read, R.J., Richardson, D.C., et al. (2012). Graphical tools for macromolecular crystallography in PHENIX. J. Appl. Crystallogr. *45*, 581–586.

Feng, Y., Wang, Y., Zhu, Z., Li, W., Sussman, R.T., Randall, M., Bosse, K.R., Maris, J.M., and Dimitrov, D.S. (2016). Differential killing of CD56-expressing

cells by drug-conjugated human antibodies targeting membrane-distal and membrane-proximal non-overlapping epitopes. MAbs *8*, 799–810.

Fibriansah, G., Tan, J.L., Smith, S.A., de Alwis, R., Ng, T.S., Kostyuchenko, V.A., Jadi, R.S., Kukkaro, P., de Silva, A.M., Crowe, J.E., et al. (2015). A highly potent human antibody neutralizes dengue virus serotype 3 by binding across three surface proteins. Nat. Commun. *6*, 6341.

Gao, R., Cao, B., Hu, Y., Feng, Z., Wang, D., Hu, W., Chen, J., Jie, Z., Qiu, H., Xu, K., et al. (2013). Human infection with a novel avian-origin influenza A (H7N9) virus. N. Engl. J. Med. *368*, 1888–1897.

Geisbert, T.W., Mire, C.E., Geisbert, J.B., Chan, Y.P., Agans, K.N., Feldmann, F., Fenton, K.A., Zhu, Z., Dimitrov, D.S., Scott, D.P., et al. (2014). Therapeutic treatment of Nipah virus infection in nonhuman primates with a neutralizing human monoclonal antibody. Sci. Transl. Med. *6*, 242ra82.

Gerhard, W., Yewdell, J., Frankel, M.E., and Webster, R. (1981). Antigenic structure of influenza virus haemagglutinin defined by hybridoma antibodies. Nature *290*, 713–717.

Henry Dunand, C.J., Leon, P.E., Kaur, K., Tan, G.S., Zheng, N.Y., Andrews, S., Huang, M., Qu, X., Huang, Y., Salgado-Ferrer, M., et al. (2015). Preexisting human antibodies neutralize recently emerged H7N9 influenza strains. J. Clin. Invest. *125*, 1255–1268.

Hobson, D., Curry, R.L., Beare, A.S., and Ward-Gardner, A. (1972). The role of serum haemagglutination-inhibiting antibody in protection against challenge infection with influenza A2 and B viruses. J. Hyg. (Lond) *70*, 767–777.

Hoot, S., McGuire, A.T., Cohen, K.W., Strong, R.K., Hangartner, L., Klein, F., Diskin, R., Scheid, J.F., Sather, D.N., Burton, D.R., et al. (2013). Recombinant HIV envelope proteins fail to engage germline versions of anti-CD4bs bNAbs. PLoS Pathog. *9*, e1003106.

Hou, D.N., Ying, T.L., Wang, L.L., Chen, C.C., Lu, S.H., Wang, Q., Seeley, E., Xu, J.Q., Xi, X.H., Li, T., et al. (2016). Immune repertoire diversity correlated with mortality in avian influenza A (H7N9) virus infected patients. Sci. Rep. *6*, 33843.

Houser, K.V., Gretebeck, L., Ying, T.L., Wang, Y.P., Vogel, L., Lamirande, E.W., Bock, K.W., Moore, I.N., Dimitrov, D.S., and Subbarao, K. (2016). Prophylaxis with a Middle East respiratory syndrome coronavirus (MERS-CoV)-specific human monoclonal antibody protects rabbits from MERS-CoV infection. J. Infect. Dis. *213*, 1557–1561.

Huang, C.C., Venturi, M., Majeed, S., Moore, M.J., Phogat, S., Zhang, M.Y., Dimitrov, D.S., Hendrickson, W.A., Robinson, J., Sodroski, J., et al. (2004). Structural basis of tyrosine sulfation and VH-gene usage in antibodies that recognize the HIV type 1 coreceptor-binding site on gp120. Proc. Natl. Acad. Sci. USA *101*, 2706–2711.

Huang, J., Ofek, G., Laub, L., Louder, M.K., Doria-Rose, N.A., Longo, N.S., Imamichi, H., Bailer, R.T., Chakrabarti, B., Sharma, S.K., et al. (2012). Broad and potent neutralization of HIV-1 by a gp41-specific human antibody. Nature *491*, 406–412.

Huang, J., Kang, B.H., Pancera, M., Lee, J.H., Tong, T., Feng, Y., Georgiev, I.S., Chuang, G.-Y., Druz, A., Doria-Rose, N.A., et al. (2014). Broad and potent HIV-1 neutralization by a human antibody that binds the gp41-120 interface. Nature *515*, 138–142.

Jardine, J., Julien, J.P., Menis, S., Ota, T., Kalyuzhniy, O., McGuire, A., Sok, D., Huang, P.S., MacPherson, S., Jones, M., et al. (2013). Rational HIV immunogen design to target specific germline B cell receptors. Science *340*, 711–716.

Jardine, J.G., Kulp, D.W., Havenar-Daughton, C., Sarkar, A., Briney, B., Sok, D., Sesterhenn, F., Ereno-Orbea, J., Kalyuzhniy, O., Deresa, I., et al. (2016). HIV-1 broadly neutralizing antibody precursor B cells revealed by germline-targeting immunogen. Science *351*, 1458–1463.

Jegaskanda, S., Reading, P.C., and Kent, S.J. (2014). Influenza-specific antibody-dependent cellular cytotoxicity: toward a universal influenza vaccine. J. Immunol. *193*, 469–475.

Kallewaard, N.L., Corti, D., Collins, P.J., Neu, U., McAuliffe, J.M., Benjamin, E., Wachter-Rosati, L., Palmer-Hill, F.J., Yuan, A.Q., Walker, P.A., et al. (2016). Structure and function analysis of an antibody recognizing all influenza A subtypes. Cell *166*, 596–608.

Keller, M.A., and Stiehm, E.R. (2000). Passive immunity in prevention and treatment of infectious diseases. Clin. Microbiol. Rev. *13*, 602–614.

Khurana, S., Chung, K.Y., Coyle, E.M., Meijer, A., and Golding, H. (2016). Antigenic fingerprinting of antibody response in humans following exposure to highly pathogenic H7N7 avian influenza virus: evidence for anti-PA-X antibodies. J. Virol. *90*, 9383–9393.

Kiso, M., Mitamura, K., Sakai-Tagawa, Y., Shiraishi, K., Kawakami, C., Kimura, K., Hayden, F.G., Sugaya, N., and Kawaoka, Y. (2004). Resistant influenza A viruses in children treated with oseltamivir: descriptive study. Lancet *364*, 759–765.

Lin, Q., Lin, Z., Chiu, A.P., and He, D. (2016). Seasonality of influenza A(H7N9) virus in china-fitting simple epidemic models to human cases. PLoS One *11*, e0151333.

Lingwood, D., McTamney, P.M., Yassine, H.M., Whittle, J.R.R., Guo, X.T., Boyington, J.C., Wei, C.J., and Nabel, G.J. (2012). Structural and genetic basis for development of broadly neutralizing influenza antibodies. Nature *489*, 566–570.

Pappas, L., Foglierini, M., Piccoli, L., Kallewaard, N.L., Turrini, F., Silacci, C., Fernandez-Rodriguez, B., Agatic, G., Giacchetto-Sasselli, I., Pellicciotta, G., et al. (2014). Rapid development of broadly influenza neutralizing antibodies through redundant mutations. Nature *516*, 418–422.

Prabakaran, P., Zhu, Z., Chen, W., Gong, R., Feng, Y., Streaker, E., and Dimitrov, D.S. (2012). Origin, diversity, and maturation of human antiviral antibodies analyzed by high-throughput sequencing. Front. Microbiol. *3*, 277.

Puligujja, P., Balkundi, S.S., Kendrick, L.M., Baldridge, H.M., Hilaire, J.R., Bade, A.N., Dash, P.K., Zhang, G., Poluektova, L.Y., Gorantla, S., et al. (2015). Pharmacodynamics of long-acting folic acid-receptor targeted ritonavir-boosted atazanavir nanoformulations. Biomaterials *41*, 141–150.

Sakai, T., Ohuchi, M., Imai, M., Mizuno, T., Kawasaki, K., Kuroda, K., and Yamashina, S. (2006). Dual wavelength imaging allows analysis of membrane fusion of influenza virus inside cells. J. Virol. *80*, 2013–2018.

Schmidt, A.G., Do, K.T., McCarthy, K.R., Kepler, T.B., Liao, H.X., Moody, M.A., Haynes, B.F., and Harrison, S.C. (2015). Immunogenic stimulus for germline precursors of antibodies that engage the influenza hemagglutinin receptor-binding site. Cell Rep. *13*, 2842–2850.

Steichen, J.M., Kulp, D.W., Tokatlian, T., Escolano, A., Dosenovic, P., Stanfield, R.L., McCoy, L.E., Ozorowski, G., Hu, X.Z., Kalyuzhniy, O., et al. (2016). HIV vaccine design to target germline precursors of glycan-dependent broadly neutralizing antibodies. Immunity *45*, 483–496.

Sun, Z.W., Zhu, Y., Wang, Q., Ye, L., Dai, Y.Y., Su, S., Yu, F., Ying, T.L., Yang, C.L., Jiang, S.B., et al. (2016). An immunogen containing four tandem 10E8 epitope repeats with exposed key residues induces antibodies that neutralize HIV-1 and activates an ADCC reporter gene. Emerg. Microbes Infect. *5*, e65.

Tan, G.S., Leon, P.E., Albrecht, R.A., Margine, I., Hirsh, A., Bahl, J., and Krammer, F. (2016). Broadly-reactive neutralizing and non-neutralizing antibodies directed against the H7 influenza virus hemagglutinin reveal divergent mechanisms of protection. PLoS Pathog. *12*, e1005578.

Tang, X.C., Agnihothram, S.S., Jiao, Y., Stanhope, J., Graham, R.L., Peterson, E.C., Avnir, Y., Tallarico, A.S., Sheehan, J., Zhu, Q., et al. (2014). Identification of human neutralizing antibodies against MERS-CoV and their role in virus adaptive evolution. Proc. Natl. Acad. Sci. USA *111*, E2018–E2026.

Tharakaraman, K., Jayaraman, A., Raman, R., Viswanathan, K., Stebbins, N.W., Johnson, D., Shriver, Z., Sasisekharan, V., and Sasisekharan, R. (2013). Glycan receptor binding of the influenza A virus H7N9 hemagglutinin. Cell *153*, 1486–1493.

Tharakaraman, K., Subramanian, V., Viswanathan, K., Sloan, S., Yen, H.L., Barnard, D.L., Leung, Y.H.C., Szretter, K.J., Koch, T.J., Delaney, J.C., et al. (2015). A broadly neutralizing human monoclonal antibody is effective against H7N9. Proc. Natl. Acad. Sci. USA *112*, 10890–10895.

Thornburg, N.J., Zhang, H., Bangaru, S., Sapparapu, G., Kose, N., Lampley, R.M., Bombardi, R.G., Yu, Y.C., Graham, S., Branchizio, A., et al. (2016). H7N9 influenza virus neutralizing antibodies that possess few somatic mutations. J. Clin. Invest. *126*, 1482–1494.

van Doremalen, N., Falzarano, D., Ying, T., de Wit, E., Bushmaker, T., Feldmann, F., Okumura, A., Wang, Y., Scott, D.P., Hanley, P.W., et al. (2017). Efficacy of antibody-based therapies against Middle East respiratory syndrome coronavirus (MERS-CoV) in common marmosets. Antiviral Res *143*, 30–37.

Wang, J., Chen, Z., Bao, L., Zhang, W., Xue, Y., Pang, X., Zhang, X., Qin, C., and Jin, Q. (2015a). Characterization of two human monoclonal antibodies neutralizing influenza A H7N9 viruses. J. Virol. *89*, 9115–9118.

Wang, Q., Bi, W.W., Zhu, X.J., Li, H.Y., Qi, Q.Q., Yu, F., Lu, L., and Jiang, S.B. (2015b). Nonneutralizing antibodies induced by the HIV-1 gp41 NHR domain gain neutralizing activity in the presence of the HIV fusion inhibitor enfuvirtide: a potential therapeutic vaccine strategy. J. Virol. *89*, 6960–6964.

Xiong, X., Martin, S.R., Haire, L.F., Wharton, S.A., Daniels, R.S., Bennett, M.S., McCauley, J.W., Collins, P.J., Walker, P.A., Skehel, J.J., et al. (2013). Receptor binding by an H7N9 influenza virus from humans. Nature *499*, 496–499.

Xu, K., Rockx, B., Xie, Y., DeBuysscher, B.L., Fusco, D.L., Zhu, Z., Chan, Y.P., Xu, Y., Luu, T., Cer, R.Z., et al. (2013). Crystal structure of the Hendra virus attachment G glycoprotein bound to a potent cross-reactive neutralizing human monoclonal antibody. PLoS Pathog. *9*, e1003684.

Yang, H., Carney, P.J., Chang, J.C., Villanueva, J.M., and Stevens, J. (2013). Structural analysis of the hemagglutinin from the recent 2013 H7N9 influenza virus. J. Virol. *87*, 12433–12446.

Ye, Z.W., Yuan, S., Poon, K.M., Wen, L., Yang, D., Sun, Z., Li, C., Hu, M., Shuai, H., Zhou, J., et al. (2017). Antibody-dependent cell-mediated cytotoxicity epitopes on the hemagglutinin head region of pandemic H1N1 influenza virus play detrimental roles in H1N1-infected mice. Front. Immunol. *8*, 317.

Yen, H.L., McKimm-Breschkin, J.L., Choy, K.T., Wong, D.D.Y., Cheung, P.P.H., Zhou, J., Ng, I.H., Zhu, H., Webby, R.J., Guan, Y., et al. (2013). Resistance to neuraminidase inhibitors conferred by an R292K mutation in a human influenza virus H7N9 isolate can be masked by a mixed R/K viral population. MBio *4*, http://dx.doi.org/10.1128/mBio.00396-13.

Ying, T., Du, L., Ju, T.W., Prabakaran, P., Lau, C.C., Lu, L., Liu, Q., Wang, L., Feng, Y., Wang, Y., et al. (2014a). Exceptionally potent neutralization of Middle East respiratory syndrome coronavirus by human monoclonal antibodies. J. Virol. *88*, 7796–7805.

Ying, T.L., Feng, Y., Wang, Y.P., Chen, W.Z., and Dimitrov, D.S. (2014b). Monomeric IgG1 Fc molecules displaying unique Fc receptor interactions that are exploitable to treat inflammation-mediated diseases. Mabs *6*, 1201–1210.

Ying, T.L., Prabakaran, P., Du, L.Y., Shi, W., Feng, Y., Wang, Y.P., Wang, L.S., Li, W., Jiang, S.B., Dimitrov, D.S., et al. (2015). Junctional and allele-specific residues are critical for MERS-CoV neutralization by an exceptionally potent germline-like antibody. Nat. Commun. *6*, 8223.

Zhou, T., Georgiev, I., Wu, X., Yang, Z.Y., Dai, K., Finzi, A., Kwon, Y.D., Scheid, J.F., Shi, W., Xu, L., et al. (2010). Structural basis for broad and potent neutralization of HIV-1 by antibody VRC01. Science *329*, 811–817.

Zhou, T., Zhu, J., Wu, X., Moquin, S., Zhang, B., Acharya, P., Georgiev, I.S., Altae-Tran, H.R., Chuang, G.Y., Joyce, M.G., et al. (2013). Multidonor analysis reveals structural elements, genetic determinants, and maturation pathway for HIV-1 neutralization by VRC01-class antibodies. Immunity *39*, 245–258.

Zhu, Z., Dimitrov, A.S., Bossart, K.N., Crameri, G., Bishop, K.A., Choudhry, V., Mungall, B.A., Feng, Y.R., Choudhary, A., Zhang, M.Y., et al. (2006). Potent neutralization of Hendra and Nipah viruses by human monoclonal antibodies. J. Virol. *80*, 891–899.

Zhu, Z., Chakraborti, S., He, Y., Roberts, A., Sheahan, T., Xiao, X., Hensley, L.E., Prabakaran, P., Rockx, B., Sidorov, I.A., et al. (2007). Potent cross-reactive neutralization of SARS coronavirus isolates by human monoclonal antibodies. Proc. Natl. Acad. Sci. USA *104*, 12123–12128.

Zhu, Z., Bossart, K.N., Bishop, K.A., Crameri, G., Dimitrov, A.S., McEachern, J.A., Feng, Y., Middleton, D., Wang, L.F., Broder, C.C., et al. (2008). Exceptionally potent cross-reactive neutralization of Nipah and Hendra viruses by a human monoclonal antibody. J. Infect. Dis. *197*, 846–853.

Zuo, T., Sun, J., Wang, G., Jiang, L., Zuo, Y., Li, D., Shi, X., Liu, X., Fan, S., Ren, H., et al. (2015). Comprehensive analysis of antibody recognition in convalescent humans from highly pathogenic avian influenza H5N1 infection. Nat. Commun. *6*, 8855.

STAR★METHODS

KEY RESOURCES TABLE

REAGENT or RESOURCE	SOURCE	IDENTIFIER
Antibodies		
HRP-conjugated mouse anti-Flag	Sigma-Aldrich	Cat# A8592; RRID: AB_439702
Anti-M13-horseradish peroxidase (HRP) polyclonal antibody	Pharmacia	Cat# 27-9421; RRID: AB_2616587
Anti-Influenza A Virus Nucleoprotein antibody	Abcam	Cat# ab20343; RRID: AB_445525
Alexa Fluor 647 conjugated goat anti-human IgG	Thermo Fisher	Cat# A-21445; RRID: AB_141843
Anti-tumor human monoclonal antibody m610.27	This paper	N/A
Anti-HBV human monoclonal antibody G12	This paper	N/A
CR9114 IgG	This paper	N/A
Bacterial and Virus Strains		
H7N3 A/RT/NJ65/85	CDC	N/A
H7N4 A/EM/Korea/W266/2007	Dr. Young-Ki Choi at Chungbuk National University, Republic of Korea	N/A
H7N9 A/Shanghai/4664T/2013	Shanghai Public Health Clinical Center, Fudan University, China	N/A
H7N9 A/Shanghai/2/2013	CDC	N/A
Biological Samples		
Human cord blood	National Disease Research Interchange	http://www.ndriresource.org/
Rabbit polyclonal sera	This paper	N/A
Sheep polyclonal sera	This paper	N/A
Chemicals, Peptides, and Recombinant Proteins		
Bafilomycin A1	Sigma-Aldrich	Cat# B1793
32% Paraformaldehyde	Electron Microscopy Sciences	Cat# 15714-S
Octadecyl Rhodamine B Chloride (R18)	Thermo Fisher	Cat# O246
3,3'-Dioctadecyl-5,5'-Di(4-Sulfonphenyl) Oxacarbocyanine, Sodium Salt (SP-DiOC18(3))	Thermo Fisher	Cat# D7778
Ni-NTA column	GE Healthcare	Cat# 17-5318-02
Protein A affinity chromatography	GE Healthcare	Cat# 17-0780-01
HiLoad 16/60 Superdex 200 column	GE Healthcare	Cat# 28990944
HA protein:H1N1 (A/California/04/2009)	Sinobiological Inc.	Cat# 11055-V08B
HA protein:H3N2 (A/Aichi/2/1968)	Sinobiological Inc.	Cat# 11707-V08B
HA protein:H5N1 (A/Hongkong/213/2003)	Sinobiological Inc.	Cat# 11713-V08B
HA protein:H7N7 (A/Netherlands/219/03)	Sinobiological Inc.	Cat# 11082-V08B
HA protein:H7N9 (A/Shanghai/1/2013)	Sinobiological Inc.	Cat# 40104-V08B
HA protein:H7N9 (A/Shanghai/2/2013)	Sinobiological Inc.	Cat# 40239-V08B
HA protein:H10N8 (A/Jiangxi-Donghu/346/2013)	Sinobiological Inc.	Cat# 40359-V08B
HA protein:H15N8 (A/duck/AUS/341/1983)	Sinobiological Inc.	Cat# 11720-V08H
Critical Commercial Assays		
ADCC Reporter Bioassay kit	Promega	Cat# G7015
CytoTox-ONE Homogeneous Membrane Integrity Assay	Promega	Cat# G7890
Deposited Data		
H7N9 HA1-m826 complex structure	This paper	PDB: 5VAG
Experimental Models: Cell Lines		
293T	ATCC	Cat# CRL-11268
MDCK	ATCC	Cat# PTA-6500

(*Continued on next page*)

Continued

REAGENT or RESOURCE	SOURCE	IDENTIFIER
Expi293 Expression System	Thermo Fisher	Cat# A14635
Sf9 insect cells	Thermo Fisher	Cat# B82501
Experimental Models: Organisms/Strains		
BALB/c mice (6-8 weeks old)	Changzhou Cavens Laboratory Animal Ltd.	Certificate# 201605048
Recombinant DNA		
HA gene: A/Shanghai/2/2013	Genscript	N/A
pSecTag2B expression vector	Thermo Fisher	Cat# V90020
pAcGP67a	BD Biosciences	Cat# 554759
pCMV3-H7N9-HA-GFPSpark	Sinobiological Inc.	Cat# VG40103-ACG
Software and Algorithms		
IMGT/High V-QUEST (version1.5.1)	IMGT	www.imgt.org
HKL3000 program	HKL Research, Inc.	N/A
ForteBio Data Analysis software	Pall ForteBio LLC	N/A
Other		
M13KO7 helper phages	Thermo Fisher	Cat# 18311019

CONTACT FOR REAGENT AND RESOURCE SHARING

Further information and requests for resources and reagents may be directed to and will be fulfilled by the Lead Contact, Tianlei Ying (tlying@fudan.edu.cn).

EXPERIMENTAL MODEL AND SUBJECT DETAILS

Murine Lethal Challenge Model

Specific-pathogen-free female BALB/c mice (6-8 weeks old) were purchased from the Changzhou Cavens Laboratory Animal Ltd. (Changzhou, China). The animals weighed 18.0 g ± 2.0 g, and five mice were housed in one individually ventilated cage. All mice were bred and housed in Biosafety Level-3 (BSL-3) under controlled conditions of humidity (70 ± 10%) and temperature (23 ± 2°C). The animal studies were reviewed and approved by the Ethics Committee of the School of Basic Medical Sciences at Fudan University (Permit Number: 20160621). Each group of six mice received a dose of 0.5 mg or 1 mg of purified antibody intraperitoneally 12 h before (prophylactic group) virus exposure, or 12 h after (therapeutic group) virus exposure. The mice were injected with PBS in the control group. The mice were weighed for 14 days and checked daily in order to monitor weight loss and survival.

Cells and Viruses

HEK293T (293T) and Madin-Darby canine kidney (MDCK) cells were obtained from the American Type Culture Collection (ATCC, #CRL-11268 for 293T, female; #PTA-6500 for MDCK, female) and cultured in Dulbecco's modified Eagle's medium (DMEM) supplemented with 10% fetal bovine serum (FBS) in 37°C, 5% CO_2 atmosphere. The H7N9 virus used in the animal study was A/Shanghai/4664T/2013 was obtained from Shanghai Public Health Clinical Center and stored at -80°C in a BSL-3 laboratory (Fudan University). A/Shanghai/4664T/2013 has very similar sequence to that of A/Shanghai/2/2013 with only a single point mutation (Y282H). The H7N3 A/RT/NJ65/85 and H7N9 A/Shanghai/2/2013 viruses used in the neutralization assay were vaccine strain viruses generated by reverse genetics obtained from CDC. The H7N9 virus titer was expressed as 50% tissue culture infection dose ($TCID_{50}$). In brief, the virus was serially diluted 10-fold. The diluted virus samples were then added to MDCK cells in 96-well plates, which were incubated at 37 °C for 3 days. The $TCID_{50}$ values were measured by determining CPE and were calculated by the Reed-Muench method. The H7N4 virus used in this study was A/EM/Korea/W266/2007, which was generously provided by Dr. Young-Ki Choi at Chungbuk National University, Republic of Korea.

METHOD DETAILS

Ethics Statement

The animal studies were reviewed and approved by the Ethics Committee of the School of Basic Medical Sciences at Fudan University (Permit Number: 20160621) in accordance with the animal ethics guidelines of the Chinese National Health and Medical Research Council (NHMRC). The cord blood samples were provided by National Disease Research Interchange (NDRI, Philadelphia, PA) with approval of institutional research board and donor consent.

Expression and Purification of Viral HA

The baculovirus-expressed H1N1 (A/California/04/2009), H3N2 (A/Aichi/2/1968), H5N1 (A/Hongkong/213/2003), H7N7 (A/Netherlands/219/03), H7N9 (A/Shanghai/1/2013, A/Shanghai/2/2013), H10N8 (A/Jiangxi-Donghu/346/2013) and the human cell-expressed H15N8 (A/duck/AUS/341/1983) HA proteins were purchased from Sinobiological Inc. (Beijing, China). The HA1 gene of A/Shanghai/2/2013 was synthesized (Genscript, Nanjing, China), fused with the Fc fragment of human IgG1 and a C-terminal Avi-tag (GLNDIFEAQKIEWHE), and cloned into pSecTag2B expression vector (Thermo Fisher). The recombinant plasmid HA1-Fc-Avi was transfected into Expi293 cells (Thermo Fisher) for transient expression and used for biopanning. The baculovirus-expressed HA1 was produced by cloning synthesized A/Shanghai/2/2013 H7N9 HA1 gene adjacent to a C-terminal 6-His tag into pAcGP67a vector (BD Biosciences) and expressed in Sf9 insect cells according to the manufacturer's instructions. The trimeric HA was generated by fusing a T4 phage fibritin-derived trimeric foldon (GYIPEAPRDGQAYVRKDGEWVLLSTFL) to the C-terminal of synthesized A/Shanghai/2/2013 H7N9 HA gene (Genscript), and transiently expressed using Expi293 Expression System (Thermo Fisher). The recombinant proteins were purified on Ni-NTA column or by Protein A affinity chromatography (GE Healthcare, Piscataway, NJ) for proteins with Fc tag, according to the manufacturer's instructions.

Antibody Screening from Phage Library

The large phage-display naïve human antigen-binding fragment (Fab) library was constructed by using PBMC cDNA from 40 healthy volunteers as the templates for cloning the expressed antibody gene repertoire. Panning protocols were essentially carried out as described previously (Ying et al., 2014a). Briefly, one aliquot each of the frozen library phage stocks was precipitated with 5% polyethylene glycol (PEG) 8000-NaCl (20% PEG 8000, 2.5 M NaCl) and re-suspended in PBS. The recombinant biotinylated HA from the A/Shanghai/1/2013 H7N9 isolate (HA-SH1) was used for the first panning of the antibody library and then biotinylated Fc-fused HA1 from the A/Shanghai/2/2013 isolate (HA1-SH2) for four more rounds, which were immobilized on streptavidin-coated magnetic beads (Invitrogen). About 10^{12} phage particles were used for each biopanning. Phages from library were pre-blocked in 3% milk powder (w/v) in PBS (MPBS) and incubated with the biotinylated antigen in 1% MPBS for 30 min and then incubated with streptavidin-coated magnetic beads for 1.5 h. After washes with PBST (PBS buffer supplemented with 0.05% Tween 20), bound phages were used to infect mid-log phase E. *coli* TG1 bacteria at 37°C for 1 h. Then, TG1 bacteria were grown in 2×YT medium containing 100 μg/ml ampicillin and 2% (w/v) glucose at 37°C and 250 rpm. After 2 h, the cells were infected with M13KO7 helper phages (Thermo Fisher) for 45 min at room temperature. The infected cells were harvested and re-suspended into 2×YT medium supplemented with 100 μg/ml ampicillin and 100 μg/ml kanamycin, followed by incubation overnight at 30°C and 220 rpm. The phages were precipitated from culture supernatant with PEG8000-NaCl and re-suspended in sterile PBS for subsequent panning. The enrichment for antigen-specific phages after each round of panning was assessed by polyclonal phage enzyme-linked immunosorbent assay (ELISA). Positive clones expressing Fab were identified from the 4^{th} and 5^{th} rounds of panning by using monoclonal phage ELISA.

Enzyme-linked Immunosorbent Assay

Corning half-area 96-well plates (Sigma-Aldrich) were coated with viral HA at 100 ng/well in PBS overnight at 4°C and blocked with 3% milk powder (w/v) in PBS buffer at 37°C. For phage ELISA, phage from each round of panning (polyclonal phage ELISA) or clones randomly picked from the fourth and fifth rounds of panning (monoclonal phage ELISA) were incubated with immobilized antigen. Bound phages were detected with anti-M13-horseradish peroxidase (HRP) polyclonal antibody (Pharmacia, Piscataway, NJ). For the soluble Fab binding assay, serially diluted antibodies were added and incubated for 1.5 h at 37°C. HRP-conjugated mouse anti-Flag (Sigma-Aldrich) was used for detection. Enzymatic activity was measured with the subsequent addition of substrate ABTS, and signal reading was carried out at 405 nm. A minimum of 3 independent experiments was performed.

Expression and Purification of m826 Fab and IgG Formats

Fab expression was performed in *E. coli* HB2151 bacterial culture according to the protocol in reference and purified on Ni-NTA column (Ying et al., 2014a). For conversion and preparation of IgG1, the heavy and light chains of Fabs were amplified and re-cloned into the pDR12 vector. The m826 IgG was expressed transiently using Expi293 Expression System (Thermo Fisher) according to the manufacturer's instructions and purified by Protein A affinity chromatography (GE Healthcare). Proteins were dialyzed into PBS. Purity was estimated as >95% by SDS-PAGE, and protein concentration was measured spectrophotometrically.

Biolayer Interferometry Binding Assays

The binding affinity of H7 HA, H7 HA1, H1 HA or H3 HA protein with m826 mAb was monitored by BLI using an Octet-Red96 device (Pall ForteBio). Briefly, m826 mAb at 30 μg/ml buffered in sodium acetate (pH 5.0) was loaded onto activated AR2G biosensors until saturation, typically for 300 s, and then incubated with 3-fold serial dilutions of viral HA and HA1 in running buffer with pH 7.4 or 5.0. Association and dissociation were measured at 37°C and fitted using ForteBio Data Analysis software.

Next-generation Sequencing

As a source for amplification of antibody gene fragments, cDNA was reverse transcripted from the total RNA extracted from B lymphocytes of 33 healthy adult donors or 10 newborn babies as described previously (Ying et al., 2014a). Cord blood of newborn babies was received from the NDRI, and care was taken not to contaminate the samples with maternal blood. Cloning of VH cDNA was

carried out according to methods described previously (Prabakaran et al., 2012), and the next-generation sequencing was performed using the Illumina HiSeq platform according to the manufactures' protocol. IMGT/High V-QUEST (version1.5.1) was used for sequence annotation and assignment of the V(D)J genes. Results from IMGT/High V-QUEST analysis were imported into PostgreSQL database, and Structured Query Language (SQL) was used to retrieve the data for statistical analysis.

Crystallization, Data Collection and Structure Determination

The m826 Fab:HA1 complex was formed by mixing each protein at a molar ratio of 1:1 and then further purified by size-exclusion chromatography on a HiLoad 16/60 Superdex 200 column (GE Healthcare). The purified complex was concentrated to 8 mg/ml for crystallization. Crystals were grown in the reservoir solution containing 0.2 M sodium fluoride and 20% (v/v) PEG 3350 by sitting drop vapor diffusion at 20°C. For data collection, the crystals were soaked in reservoir solution containing 20% (v/v) ethylene glycol and flash-frozen in liquid nitrogen. The X-ray (λ = 1.0 Å) diffraction data were collected at -173°C using a Rayonix MX3000HS detector at the 22-ID beamline of SER-CAT of Advanced Photon Source, Argonne National Laboratory. The X-ray data were processed using the HKL3000 program (HKL Research, Inc.). The structure was solved by molecular replacement using the PHASER program embedded in the PHENIX suite (Echols et al., 2012) with the H7N9 HA (PDB: 4LN4) and Fab antibody (PDB: 1EO8) as the search models. Programs Coot and Phenix.refine were used for model building and structure refinement. The final structure was evaluated by the validation server of wwPDB. Data collection and structure statistics are summarized in Table 1. Coordinates and structure factors have been deposited in the Protein Data Bank under accession code PDB 5VAG.

Hemagglutination Inhibition and Neutralization Assays

Hemagglutination inhibition assays were conducted with H7N9 HA as antigen and horse red blood cells as indicators using routine methods, as described previously (Hobson et al., 1972; Khurana et al., 2016). Polyclonal sera from rabbits that were immunized with the trimeric H7N7 or H7N9 HA1 domains (K23, K64, K65, K66) were used as positive controls. An unrelated anti-tumor IgG m610.27 was used as negative control.

Viral cytopathic effect (CPE)-based neutralization assay was conducted to determine the neutralizing antibody titers of mAb against live H7N3 and H7N9 viruses as previously described (Khurana et al., 2016). Polyclonal sera from rabbits immunized with H7N7 or H7N9 HA1 (K23, K64, K65, K66), or from sheep immunized with H7N9 HA1 were used as positive controls. In brief, serial 2-fold dilution of mAbs was mixed with 100 $TCID_{50}$ of H7N3 or H7N9 and incubated at 37 °C for 2 h. Next, the virus and mAb mixtures were added to MDCK cells in 96-well plates, and medium was replaced with fresh DMEM 2 h later. Viral cytopathic effect (CPE) was observed daily and recorded on Day 3 post-infection. The H7N9 neutralization experiment was performed under BSL-3 conditions. A minimum of 3 independent experiments was performed.

The immunostaining-based neutralization assay was carried out to detect the neutralizing activity of mAb against live H7N4 as previously described (Chai et al., 2017). Briefly, A549 cells were grown to confluent monolayer in black clear bottom plates (Greiner Bio-One, Frickenhausen, Germany) at 37°C for 24 h and fed with Opti-PRO SFM (Gibco, USA) prior to viral infection. H7N4 virus was diluted in Opti-PRO SFM at an MOI of 0.1 and incubated for 30 min at 37°C with 2 mg/ml of different mAbs. The mixture was inoculated to A549 cells for 16 h at 37°C in 5% CO_2 incubator, and the infection was arrested with 4% PFA. Immunostaining was conducted using influenza NP-specific mAbs (Abcam, Cambridge, UK) to detect virus-infected cells. Confocal images were acquired with the Opera High Content Screening System (Perkin Elmer, Shelton, CT) at 20 × magnification. Image analysis was performed using in-house, image-mining software.

Cell-based Binding and Viral Entry Assays

For cell-based binding assay, HEK293T cells were transfected with pCMV3-H7N9-HA-GFPSpark (Sinobiological Inc., Beijing, China), which codes full-length H7N9 A/Shanghai/2/2013 HA with a C-terminal GFP flag, using PEI method according to the manufacture's protocol. After 48 h, the cells were fixed with 4% PFA and blocked, and stained with 100 nM m826 and G12 (unrelated anti-HBV human monoclonal antibody) for 1 h. After washed, the cells were incubated with Alexa Fluor 647 conjugated goat anti-human IgG (Thermo Fisher). After washing the samples were mounted and confocal images were record with a Leica confocal microscope and processed with LAS AF Lite software.

The entry assays were performed as previously described (Banerjee et al., 2013). Briefly, A549 cells were grown in black 96-well clear plates at 37°C for 24 h. H7N4 virus was labeled with the lipophilic fluorescent dyes R18 and SP-$DiOC_{18}$(3) (Sakai et al., 2006) to monitor cell binding and membrane fusion. The labeled H7N4 virus at a MOI of 10 was incubated with 2 mg/ml of mAbs for 30 m at 37°C and then inoculated to A549 cells for 1 h at 4°C. Unbound virions were removed by washing three times with cold DPBS. Cells were refed with Opti-PRO SFM and incubated at 37°C. Cells were fixed with 4% PFA containing Hoechst 33342 at 30 mpi for cell binding and 180 mpi for membrane fusion, respectively. Neuraminidase (NA) was used as positive control to remove sialic acid residues of A549 cells that blocks attachment of viruses. Bafilomycin A1 was used as positive control for inhibition of endosome acidification in membrane fusion assay. Cells were observed under the Operetta High-Content Imaging System (Perkin Elmer) at 20 × magnification. A minimum of 3 independent experiments was performed.

ADCC Assay

The dual-luciferase reporter gene-based ADCC assay was performed using an ADCC Reporter Bioassay kit from Promega according to the manufacturer's instructions. In brief, 293 T cells expressing H7N9 HA (2.5×10^4 cells/well in 25 μl) as the target cells were

seeded in each well of a 96-well flat-bottomed culture plate. A measure of 50 μl of serially diluted antibody was added to the culture plates. As the effector cells, engineered FcγRIIIa-expressing Jurkat T lymphocytes were co-cultured with the antibody-treated target cells at 37 °C for 24 h, and the luciferase activity was then measured using luciferase assay regents and a luminescence counter (Infinite M200 Pro) (Sun et al., 2016). The PBMC-based cytotoxicity assay was performed as previously described with some modifications (Ying et al., 2014b). In brief, target 293T cells expressing H7N9 HA (1×10^4 cells/well in 25 μl) were mixed with 50 μl serially diluted antibody for 30 min. Human PBMCs, as the effector cells (5×10^5 cells/well in 25 μl), were co-cultured with antibody-treated target cells at 37 °C for 24 h. Then ADCC activity was measured using CytoTox-ONE Homogeneous Membrane Integrity Assay (Promega) according to the manufacturer's protocol. A minimum of 3 independent experiments was performed.

Histopathological Analysis

One mouse randomly selected from each group was sacrificed after Day 6 post-challenge, and lung tissues of these challenged mice were immediately fixed in 4% paraformaldehyde for 24 h and embedded in paraffin. Tissue sections 4 to 6 μM in thickness were stained with haematoxylin and eosin. Histopathological changes caused by H7N9 virus infection were examined by light microscope and lung pathology was analyzed by a pathologist blinded to the experimental design, as previously described (Chen et al., 2015; Du et al., 2013).

QUANTIFICATION AND STATISTICAL ANALYSIS

Unless otherwise stated, data analyses were performed using GraphPad Prism 7.0 software. Results were expressed as mean values with standard deviation and statistical details can be found directly in the figures or in the corresponding figure legends. Groups (n = 5) of female 6-8 week old mice were used for experiments. Investigators were blinded for histology experiments and animal identity as described above.

DATA AVAILABILITY

Atomic coordinates and structure factor amplitudes for the m826-HA1 complex have been deposited in the PDB under accession code 5VAG.